

Attitude Observability from Light Curve Measurements

Joanna C. Hinks* Richard Linares,[†] and John L. Crassidis[‡]

The observability of space object attitude from light curve data is analyzed. Light curves, which are the time-varying apparent brightness of sunlight reflected off a space object and measured by an observer, depend on the object position, attitude, surface material, shape, and other parameters. Previous work employing light curve data for shape estimation requires the availability of good attitude estimates. This paper explores the possibility of obtaining attitude information from the brightness measurements themselves. Some types of attitude estimate errors are detectable from individual brightness measurements, but other attitude errors lie in the nullspace of the Fisher information matrix and are not observable in the static case. Analytical expressions for the nullspace vectors are derived. The observability of the light curve model parameters is also briefly addressed.

I. Introduction

A major research topic in recent years has been space situational awareness, which is concerned with the identification and tracking of all space objects (SOs) in orbit around Earth. This task faces many challenges, one of the greatest of which is inadequate data due to the limited number of available sensors. Consequently, many research efforts focus on extracting as much information as possible from the data. For a given SO, it is standard to estimate position, velocity, and B^* , which is related to ballistic coefficient. Other useful information which is less commonly estimated includes surface material properties and SO shape.

Shape estimation in particular is valuable for object identification, and shape may influence an object's orbit. Some shape estimation techniques have relied on radar measurements, but these methods are typically limited to SOs that have relatively low orbits and have an area larger than the radar signal wavelength.¹⁻³ Other methods create a point cloud from a laser-radar (LADAR) three-dimensional scan, particularly as part of a filtering approach.^{4,5} Still other techniques employ pixel data from visual sensors.^{6,7} Vision-based methods typically have a high computational burden, and ground-based telescopes require high resolution.

Another possibility for shape estimation is an algorithm based on light curve data. Light curves are time-varying brightness measurements that result when sunlight reflects off of the surfaces of a moving SO and reaches an observer. Light curves have been used to estimate the size and shape of asteroids.^{8,9} In combination with thermal emissions, light curve data have been used to estimate the three-dimensional shape of an object.¹⁰ Other efforts have focused on estimation of position and attitude, and the respective rates of those quantities.^{11,12} Light curves depend on the relative positions of the Sun, SO, and observer, the orientation and size of the SO surfaces, as well as surface material properties. Consequently, estimation of any of these characteristics could potentially be improved by incorporating light curve data.

All previous efforts that apply light curve data to shape estimation have required that the SO attitude be fairly well-known in advance. This assumption is generally a poor one if the object being tracked is sufficiently unknown to require estimation of its shape. Attitude determination algorithms typically rely on measurements from onboard sensors, particularly vector measurements.¹³⁻¹⁶ When suitable onboard sensors are not available, one possible solution is to use the light curve data itself to estimate the SO attitude. The goal of this paper is to examine the observability of attitude from light curve measurements. In particular,

*Postdoctoral Assistant, Department of Mechanical & Aerospace Engineering, University at Buffalo, State University of New York, Amherst, NY, 14260-4400. Email: jchinks@buffalo.edu. Member AIAA.

[†]Graduate Student, Department of Mechanical & Aerospace Engineering, University at Buffalo, State University of New York, Amherst, NY, 14260-4400. Email: linares2@buffalo.edu, Student Member AIAA.

[‡]CUBRC Professor in Space Situational Awareness, Department of Mechanical & Aerospace Engineering, University at Buffalo, State University of New York, Amherst, NY, 14260-4400. Email: johnc@buffalo.edu. Associate Fellow AIAA.

static observability is investigated analytically to determine what types of attitude errors can be detected from a single measurement of apparent brightness.

The remaining sections of this paper are organized as follows: Section II presents the assumed mathematical models for the SO shape, location, and attitude, as well as the assumed model for the light curve observations. In Section III, some observability concepts are reviewed and applied to the problem of interest. Section IV outlines necessary calculations for the observability analysis and discusses the results of those calculations from a qualitative perspective. Section V examines the observability of the light curve model parameters, and Section VI draws some conclusions.

II. Light Curve Measurement Model

The mathematical model for the light curve measurements requires two sets of equations. First, the SO shape, relative location and orientation must be characterized. Second, equations must be developed to describe the way that sunlight reflects off the SO and reaches an observer.

A. Shape Model and Scenario Configuration

Each SO is assumed to be a rigid body, with an outer surface consisting of a finite number of flat plates or facets. The i^{th} facet has a total area $\mathcal{A}_{(i)}$. Its orientation relative to the SO body (B) frame is given by the unit-length basis vectors $\mathbf{u}_{u(i)}^B$, $\mathbf{u}_{v(i)}^B$, and $\mathbf{u}_{n(i)}^B$. The vector $\mathbf{u}_{n(i)}^B$ points outward along the surface normal, whereas $\mathbf{u}_{u(i)}^B$ and $\mathbf{u}_{v(i)}^B$ lie in the plane of the facet. This orthonormal triad of vectors is constructed such that $\mathbf{u}_{u(i)}^B \times \mathbf{u}_{v(i)}^B = \mathbf{u}_{n(i)}^B$.

The relative orientation of the SO's B frame and the inertial (I) frame is described by the true attitude matrix A_{true} , such that the representations of any vector \mathbf{v} in the I and B frames are related by $\mathbf{v}^B = A_{\text{true}} \mathbf{v}^I$. The estimated attitude matrix \hat{A} differs from the true attitude by the vector of small angle errors $\delta\boldsymbol{\alpha}$:

$$\hat{A} = \exp \{ - [\delta\boldsymbol{\alpha} \times] \} A_{\text{true}} \approx (\mathbf{I} - [\delta\boldsymbol{\alpha} \times]) A_{\text{true}} \quad (1)$$

where $[\delta\boldsymbol{\alpha} \times]$ is the standard cross product matrix formed from the error vector $\delta\boldsymbol{\alpha}$.

The positions of the SO, Sun, and observer are given in the I frame by the vectors \mathbf{R}_{SO}^I , $\mathbf{R}_{\text{sun}}^I$ and $\mathbf{R}_{\text{obs}}^I$, respectively. For the observation model, it is most convenient to work in a coordinate system centered on the SO. In such a system, the relative positions of the Sun and the observer are given by $\mathbf{r}_{\text{sun}}^I = \mathbf{R}_{\text{sun}}^I - \mathbf{R}_{\text{SO}}^I$ and $\mathbf{r}_{\text{obs}}^I = \mathbf{R}_{\text{obs}}^I - \mathbf{R}_{\text{SO}}^I$. The distance from the observer to the SO is $d = \|\mathbf{r}_{\text{obs}}^I\|$.

The light curve observation model involves $\mathbf{u}_{\text{obs}}^I$ and $\mathbf{u}_{\text{sun}}^I$, the line of sight (LOS) unit vectors formed by normalizing the position vectors $\mathbf{r}_{\text{obs}}^I$ and $\mathbf{r}_{\text{sun}}^I$. The model also requires the unit half-vector \mathbf{u}_h^I , which bisects the angle between $\mathbf{u}_{\text{obs}}^I$ and $\mathbf{u}_{\text{sun}}^I$:

$$\mathbf{u}_h^I = \frac{\mathbf{u}_{\text{obs}}^I + \mathbf{u}_{\text{sun}}^I}{\|\mathbf{u}_{\text{obs}}^I + \mathbf{u}_{\text{sun}}^I\|} \quad (2)$$

Figure 1 illustrates the surface basis vectors and LOS vectors that enter the light curve calculations.

B. Light Curve Observation Model

The apparent brightness magnitude, which is measured by the observer, is

$$m_{\text{app}} = -26.7 - 2.5 \log_{10} \left| \sum_{i=1}^N \frac{F_{\text{obs}(i)}}{C_{\text{sun,vis}}} \right| \quad (3)$$

where -26.7 is the apparent magnitude of the Sun, $C_{\text{sun,vis}} = 455 \text{W/m}^2$ is the power per square meter of visible sunlight striking the object surface, and $F_{\text{obs}(i)}$ is the fraction of the sunlight striking the i^{th} facet that is reflected. $F_{\text{obs}(i)}$ is in turn calculated as

$$F_{\text{obs}(i)} = \frac{F_{\text{sun}(i)} \mathcal{A}_{(i)} (\mathbf{u}_{\text{obs}}^I \cdot \mathbf{u}_{n(i)}^I)}{d^2} \quad (4)$$

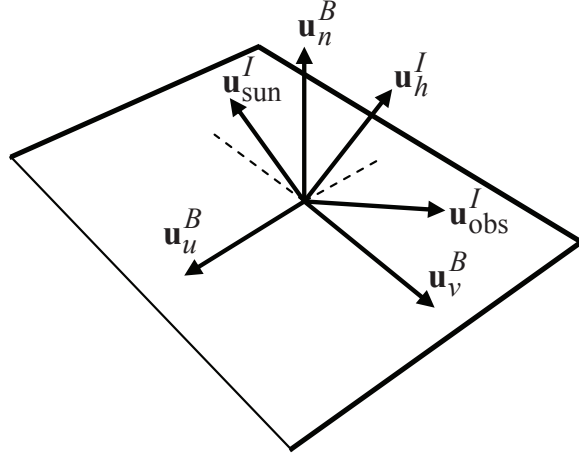


Figure 1. Reflection Geometry

where $F_{\text{sun}(i)}$ is the fraction of visible sunlight that strikes the i^{th} facet and is not absorbed.

The fraction $F_{\text{sun}(i)}$ is given by

$$F_{\text{sun}(i)} = C_{\text{sun,vis}} \rho_{\text{total}(i)} \left(\mathbf{u}_{\text{sun}}^I \cdot \mathbf{u}_{n(i)}^I \right) \quad (5)$$

In Eq. (5), $\rho_{\text{total}(i)}$ is the total bidirectional reflectance distribution function (BRDF) for the i^{th} facet, which is composed of a specular component $\rho_{\text{spec}(i)}$ and a diffuse component $\rho_{\text{diff}(i)}$:

$$\rho_{\text{total}(i)} = \rho_{\text{spec}(i)} + \rho_{\text{diff}(i)} \quad (6)$$

The BRDF used here, which is a modified version of the Phong model, is described in Refs. 17,18. The specular component of the BRDF is

$$\rho_{\text{spec}(i)} = k_{1(i)} \frac{\rho_{\text{spec,num}(i)}}{\rho_{\text{spec,den}(i)}} F_{\text{reflect}(i)} \quad (7)$$

The constant $k_{1(i)}$ is given by

$$k_{1(i)} = \frac{\sqrt{(n_{u(i)} + 1)(n_{v(i)} + 1)}}{8\pi} \quad (8)$$

where the parameters $n_{u(i)}$ and $n_{v(i)}$ are inputs to the reflection model that specify the distribution of the specular lobe in the $\mathbf{u}_{u(i)}^B$ and $\mathbf{u}_{v(i)}^B$ directions. For this analysis they are assumed to be $n_{u(i)} = n_{v(i)} = 1000$. The Fresnel reflectance $F_{\text{reflect}(i)}$ is approximated as¹⁹

$$F_{\text{reflect}(i)} = R_{\text{spec}(i)} + (1 - R_{\text{spec}(i)}) (1 - \mathbf{u}_{\text{sun}}^I \cdot \mathbf{u}_h^I)^5 \quad (9)$$

where $R_{\text{spec}(i)}$ is the surface material's specular reflectance at normal incidence. The numerator and denominator specular components $\rho_{\text{spec,num}(i)}$ are

$$\rho_{\text{spec,num}(i)} = \left(\mathbf{u}_h^I \cdot \mathbf{u}_{n(i)}^I \right)^z \quad (10a)$$

$$\rho_{\text{spec,den}(i)} = \left(\mathbf{u}_{\text{obs}}^I \cdot \mathbf{u}_{n(i)}^I \right) + \left(\mathbf{u}_{\text{sun}}^I \cdot \mathbf{u}_{n(i)}^I \right) - \left(\mathbf{u}_{\text{obs}}^I \cdot \mathbf{u}_{n(i)}^I \right) \left(\mathbf{u}_{\text{sun}}^I \cdot \mathbf{u}_{n(i)}^I \right) \quad (10b)$$

where the numerator exponent z is

$$z = \frac{n_{u(i)} \left(\mathbf{u}_h^I \cdot \mathbf{u}_{u(i)}^I \right)^2 + n_{v(i)} \left(\mathbf{u}_h^I \cdot \mathbf{u}_{v(i)}^I \right)^2}{1 - \left(\mathbf{u}_h^I \cdot \mathbf{u}_{n(i)}^I \right)^2} \quad (11)$$

Note that when $n_{u(i)} = n_{v(i)} = n_{uv(i)}$, Eq. (11) simplifies to the attitude-independent expression $z = n_{uv(i)}$. The diffuse part of the BRDF for the i^{th} facet is

$$\rho_{\text{diff}(i)} = k_{2(i)} \left[1 - \left(1 - \frac{\mathbf{u}_{\text{obs}}^I \cdot \mathbf{u}_{n(i)}^I}{2} \right)^5 \right] \left[1 - \left(1 - \frac{\mathbf{u}_{\text{sun}}^I \cdot \mathbf{u}_{n(i)}^I}{2} \right)^5 \right] \quad (12)$$

In Eq. (12), the constant $k_{2(i)}$ is computed as

$$k_{2(i)} = \left(\frac{28R_{\text{diff}(i)}}{23\pi} \right) (1 - R_{\text{spec}(i)}) \quad (13)$$

where $R_{\text{diff}(i)}$ is the diffuse reflectance of facet i .

The only dependence of the brightness measurement equations on attitude is through the vectors $\mathbf{u}_{n(i)}^I$, $\mathbf{u}_{u(i)}^I$ and $\mathbf{u}_{v(i)}^I$, which specify the orientation of the reflecting facet. The SO shape model defines these vectors in the body (B) frame, and they must be rotated by the estimated attitude matrix \hat{A} before they can be used in the model equations. Qualitatively, brightness m_{app} is greatest when the SO attitude is such that the surface normal $\mathbf{u}_{n(i)}^I$ exactly aligns with the bisector \mathbf{u}_h^I ; at this angle specular reflection dominates and the light is said to “glint” off the SO facet directly towards the observer. As the SO attitude varies relative to the glint direction, brightness decreases significantly. Figure 2 shows the value of m_{app} for a variety of SO attitudes centered on the attitude at which glint occurs. Note that m_{app} is defined such that lower numerical values correspond to brighter reflections and vice versa. The horizontal axes are the projections of the surface normal vector $\mathbf{u}_{n(i)}^I$ onto the plane normal to \mathbf{u}_h^I in the pitch and roll directions, respectively. The SO/observer configuration for this example, as well as for the figures in later sections, is representative of an object near GEO orbit, but the general shape of the plot does not change significantly with orbit radius.

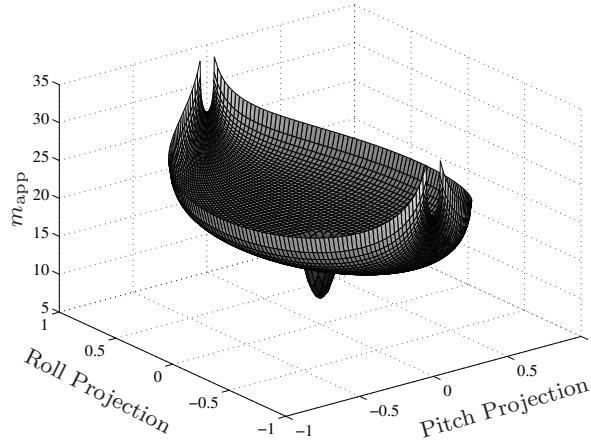


Figure 2. Apparent Brightness as a Function of Attitude

III. Observability and the Fisher Information Matrix

The goal of the present study is to explore the observability of attitude from light curve measurements. In other words, it seeks to determine what information about attitude is contained within each observation of the brightness m_{app} . Note that the restriction to a single observation makes this a *static* observability analysis; it does not directly address the performance of a filter acting on a series of brightness measurements with an assumed model of the SO dynamics. The present analysis is also a *local* observability analysis. That is, given some *a priori* estimate of the SO attitude, it investigates whether small errors in the attitude estimate relative to the true attitude can be detected in the observations.

Attitude observability is studied via the Fisher information matrix (FIM).²⁰ The FIM is defined as

$$F = \mathbb{E} \left\{ \left[\frac{\partial}{\partial \mathbf{x}} \ln p(\mathbf{y}|\mathbf{x}) \right]^T \left[\frac{\partial}{\partial \mathbf{x}} \ln p(\mathbf{y}|\mathbf{x}) \right] \right\} \quad (14)$$

where $p(\mathbf{y}|\mathbf{x})$ is the likelihood function for the measurement \mathbf{y} given the state \mathbf{x} . The significance of the Fisher information matrix is that it provides a metric of the information about the state \mathbf{x} contained in the observation \mathbf{y} . Its inverse defines the Cramér-Rao lower bound²⁰ on the estimation error covariance P :

$$P = \mathbb{E} \left\{ (\mathbf{x} - \hat{\mathbf{x}})(\mathbf{x} - \hat{\mathbf{x}})^T \right\} \geq F^{-1} \quad (15)$$

If the measurement model has the form $\mathbf{y} = \mathbf{h}(\mathbf{x}) + \boldsymbol{\nu}$, where the measurement noise $\boldsymbol{\nu}$ is distributed as a Gaussian with zero mean and covariance R , then the FIM calculations reduce to:

$$F = \left(\frac{\partial \mathbf{h}(\mathbf{x})}{\partial \mathbf{x}} \right)^T R^{-1} \left(\frac{\partial \mathbf{h}(\mathbf{x})}{\partial \mathbf{x}} \right) \quad (16)$$

For the present analysis, the brightness measurements m_{app} are assumed to have Gaussian noise with zero mean and a variance of σ^2 . The state vector of interest is the 3×1 vector of attitude errors $\boldsymbol{\delta\alpha}$, so $\partial m_{\text{app}}/\partial \boldsymbol{\delta\alpha}$ for a single measurement of m_{app} has dimension 1×3 , and the FIM is a 3×3 matrix. Because the FIM is computed as the outer product of two vectors, it has a rank of 1 and two zero-valued eigenvalues. Its two nullspace vectors represent attitude error directions that are unobservable from a single observation. Section IV presents the partial derivatives that enter the calculation of $\partial m_{\text{app}}/\partial \boldsymbol{\delta\alpha}$, and seeks to determine the nullspace directions for an individual measurement.

IV. Attitude Observability

The goal of the following analysis is to determine what attitude information is provided by a single light curve measurement. To that end, the sensitivity matrix $\partial m_{\text{app}}/\partial \boldsymbol{\delta\alpha}$ is computed. This 1×3 matrix plays the role of the partial derivative $\partial \mathbf{h}(\mathbf{x})/\partial \mathbf{x}$ in the FIM calculation of Eq. (16).

Starting with Eq. (3), the partial derivative $\partial m_{\text{app}}/\partial \boldsymbol{\delta\alpha}$ is calculated by repeated applications of the chain rule to the light curve model equations of Section II. Recall that attitude dependence arises in these equations only through the unit vectors $\mathbf{u}_{n(i)}^T$, $\mathbf{u}_{u(i)}^T$ and $\mathbf{u}_{v(i)}^T$, which specify the orientation of the reflecting i^{th} facet. The SO shape model defines these vectors in body (B) coordinates, but they must be rotated by the attitude matrix A_{true} to transform them to inertial coordinates before they can be used in the model equations. The true attitude A_{true} is written in terms of the estimated attitude \hat{A} and the attitude error $\boldsymbol{\delta\alpha}$, so the rotation introduces a dependence on $\boldsymbol{\delta\alpha}$. In the partial derivative calculations, only quantities which contain these rotated vectors have nonzero derivatives.

After performing the necessary operations, the resulting expression can be simplified by evaluating it at the point where the attitude error $\boldsymbol{\delta\alpha}$ goes to zero so that $\hat{A} = A_{\text{true}}$. Under this assumption, the partial derivative is

$$\begin{aligned} \frac{\partial m_{\text{app}}}{\partial \boldsymbol{\delta\alpha}} = \frac{-2.5}{\ln(10) \sum_{i=1}^N F_{\text{obs}(i)}} \sum_{i=1}^N F_{\text{obs}(i)} & \left[C_{n1(i)} \left(\mathbf{u}_{\text{obs}}^B \times \mathbf{u}_{n(i)}^B \right)^T + C_{n2(i)} \left(\mathbf{u}_{\text{sun}}^B \times \mathbf{u}_{n(i)}^B \right)^T \right. \\ & \left. + C_{u(i)} \left(\mathbf{u}_h^B \times \mathbf{u}_{u(i)}^B \right)^T + C_{v(i)} \left(\mathbf{u}_h^B \times \mathbf{u}_{v(i)}^B \right)^T \right] \quad (17) \end{aligned}$$

where $C_{n1(i)}$, $C_{n2(i)}$, $C_{u(i)}$, and $C_{v(i)}$ are scalars, given by

$$C_{n1(i)} = \frac{\rho_{\text{spec}(i)}}{\rho_{\text{total}(i)}} \left[\frac{z}{x_{Ai} + x_{Bi}} - \frac{1 - x_{Bi}}{x_{Ai} + x_{Bi} - x_{Ai}x_{Bi}} \right] + \frac{5k_2(i)}{2\rho_{\text{total}(i)}} \left[1 - \left(1 - \frac{x_{Bi}}{2} \right)^5 \right] \left[1 - \frac{x_{Ai}}{2} \right]^4 + \frac{1}{x_{Ai}} \quad (18a)$$

$$C_{n2(i)} = \frac{\rho_{\text{spec}(i)}}{\rho_{\text{total}(i)}} \left[\frac{z}{x_{Ai} + x_{Bi}} - \frac{1 - x_{Ai}}{x_{Ai} + x_{Bi} - x_{Ai}x_{Bi}} \right] + \frac{5k_2(i)}{2\rho_{\text{total}(i)}} \left[1 - \left(1 - \frac{x_{Ai}}{2} \right)^5 \right] \left[1 - \frac{x_{Bi}}{2} \right]^4 + \frac{1}{x_{Bi}} \quad (18b)$$

$$C_{u(i)} = 2 \left(n_{u(i)} - n_{v(i)} \right) \frac{\rho_{\text{spec}(i)} \ln(x_{ni}) x_{ui} x_{vi}^2}{\rho_{\text{total}(i)} (x_{ui}^2 + x_{vi}^2)^2} \quad (18c)$$

$$C_{v(i)} = -2 (n_{u(i)} - n_{v(i)}) \frac{\rho_{\text{spec}(i)} \ln(x_{ni}) x_{vi} x_{ui}^2}{\rho_{\text{total}(i)} (x_{ui}^2 + x_{vi}^2)^2} \quad (18d)$$

where the symbols $x_{Ai} = \mathbf{u}_{\text{obs}}^I \cdot \mathbf{u}_{n(i)}^I$, $x_{Bi} = \mathbf{u}_{\text{sun}}^I \cdot \mathbf{u}_{n(i)}^I$, $x_{ni} = \mathbf{u}_h^I \cdot \mathbf{u}_{n(i)}^I$, $x_{ui} = \mathbf{u}_h^I \cdot \mathbf{u}_{u(i)}^I$, and $x_{vi} = \mathbf{u}_h^I \cdot \mathbf{u}_{v(i)}^I$ have been defined for compactness. Note that the expression for $C_{n2(i)}$ is identical to the expression for $C_{n1(i)}$, except with x_{Ai} and x_{Bi} interchanged. Likewise, $C_{u(i)}$ and $C_{v(i)}$ are identical, except with the dot products x_{ui} and x_{vi} and the parameters $n_{u(i)}$ and $n_{v(i)}$ interchanged.

When $n_{u(i)} = n_{v(i)}$, as is assumed for this analysis, $C_{u(i)} = C_{v(i)} = 0$. Suppose also that all the reflected light comes from a single facet on the SO, so that the summations of Eq. (17) can be eliminated. If the individual scalar light curve measurements have noise with zero mean and variance σ^2 , then the FIM for a single measurement of brightness m_{app} and a single reflecting facet is given by application of Eq. (16) and some simplification:

$$\begin{aligned} F &= \frac{1}{\sigma^2} \left(\frac{\partial m_{\text{app}}}{\partial \delta \boldsymbol{\alpha}} \right)^T \left(\frac{\partial m_{\text{app}}}{\partial \delta \boldsymbol{\alpha}} \right) \\ &= \frac{1}{\sigma^2} \left(\frac{-2.5}{\ln(10)} \right)^2 \left[\mathbf{u}_{n(i)}^B \times \right] \left\{ C_{n1(i)}^2 (\mathbf{u}_{\text{obs}}^B)(\mathbf{u}_{\text{obs}}^B)^T + C_{n2(i)}^2 (\mathbf{u}_{\text{sun}}^B)(\mathbf{u}_{\text{sun}}^B)^T \right. \\ &\quad \left. + C_{n1(i)} C_{n2(i)} \left[(\mathbf{u}_{\text{obs}}^B)(\mathbf{u}_{\text{sun}}^B)^T + (\mathbf{u}_{\text{sun}}^B)(\mathbf{u}_{\text{obs}}^B)^T \right] \right\} \left[\mathbf{u}_{n(i)}^B \times \right]^T \quad (19) \end{aligned}$$

The FIM is formed by an outer product of the partial derivative vector with itself, so its nullspace is composed of two orthogonal vectors that lie in the plane orthogonal to $\partial m_{\text{app}} / \partial \delta \boldsymbol{\alpha}$. One of these nullspace vectors is aligned with $\mathbf{u}_{n(i)}^B$, as is evident from the expressions in Eqs. (17) and (19). This result makes sense: if the surface reflective properties are isotropic ($n_{u(i)} = n_{v(i)}$), rotations around the surface normal vector have no effect on brightness and are thus unobservable.

The second nullspace vector can be found by re-examining Eq. (17). Under the assumptions of an isotropic surface and zero attitude error, the remaining terms can be combined to write the partial derivative vector as a single cross product of $\mathbf{u}_{n(i)}^B$ and the sum $(C_{n1(i)} \mathbf{u}_{\text{obs}}^B + C_{n2(i)} \mathbf{u}_{\text{sun}}^B)$. Therefore, $\partial m_{\text{app}} / \partial \delta \boldsymbol{\alpha}$ must be orthogonal to this sum. The second nullspace vector is just the projection of the sum vector onto the $u - v$ plane, such that it is also orthogonal to $\mathbf{u}_{n(i)}^B$. The two-dimensional nullspace of the FIM is thus given by

$$\mathbf{n}_1 = \mathbf{u}_{n(i)}^B \quad (20a)$$

$$\mathbf{n}_2 = \frac{\beta_{u(i)} \mathbf{u}_{u(i)}^B + \beta_{v(i)} \mathbf{u}_{v(i)}^B}{\sqrt{\beta_{u(i)}^2 + \beta_{v(i)}^2}} \quad (20b)$$

where the projection scalars $\beta_{u(i)}$ and $\beta_{v(i)}$ are computed as

$$\beta_{u(i)} = C_{n1(i)} (\mathbf{u}_{\text{obs}}^B \cdot \mathbf{u}_{u(i)}^B) + C_{n2(i)} (\mathbf{u}_{\text{sun}}^B \cdot \mathbf{u}_{u(i)}^B) \quad (21a)$$

$$\beta_{v(i)} = C_{n1(i)} (\mathbf{u}_{\text{obs}}^B \cdot \mathbf{u}_{v(i)}^B) + C_{n2(i)} (\mathbf{u}_{\text{sun}}^B \cdot \mathbf{u}_{v(i)}^B) \quad (21b)$$

The amount of attitude information provided by a single measurement depends strongly on the SO attitude itself, and how sensitive the brightness m_{app} is to small changes relative to a particular attitude. One way to parameterize this ‘‘information magnitude’’ is by the (only) nonzero singular value of the FIM, which can also be computed as the square of the norm of $\partial m_{\text{app}} / \partial \delta \boldsymbol{\alpha}$, divided by the measurement variance σ^2 . This value is plotted in Fig. 3 for a variety of attitudes centered around the glint direction, as in Fig. 2. The SO/observer configuration and the horizontal axes are the same as in that figure. In Fig. 3, information magnitude is plotted on a log scale for easier visualization, with larger values corresponding to more information. Figure 4 presents an alternative visualization by plotting the magnitude of the partial derivative $\partial m_{\text{app}} / \partial \delta \boldsymbol{\alpha}$ on a linear scale. Although it has the same horizontal axes as Fig. 3, they are zoomed in so that only a small region near the glint direction is shown. From Figs. 3 and 4, it is evident that information is maximized in two regions. First, attitudes near (but not exactly at) the glint direction produce large changes in brightness for very small changes in attitude. (When $\mathbf{u}_{n(i)}^I = \mathbf{u}_h^I$ exactly, the derivative $\partial m_{\text{app}} / \partial \delta \boldsymbol{\alpha}$ goes to zero, as seen in Fig. 2.) Second, there is much information near the edges of the range of attitudes that reflect sunlight to the observer. These boundary attitudes, however, correspond to m_{app} values that are very dim in Fig. 2, so it might be harder to obtain such observations with the available sensors.

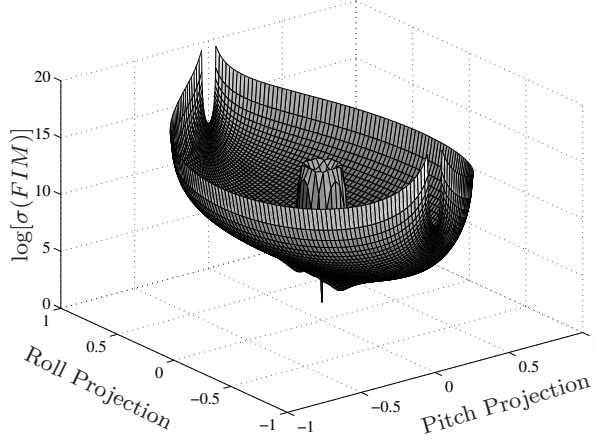


Figure 3. Information Magnitude as a Function of Attitude

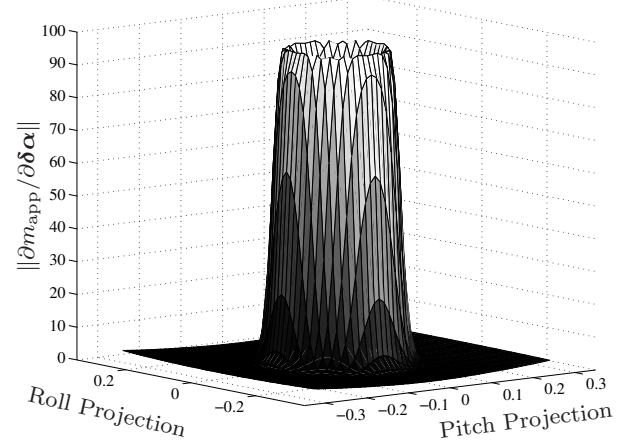


Figure 4. Partial Derivative Magnitude as a Function of Attitude

V. BRDF Model Parameter Observability

The following equations give the partial derivatives of apparent brightness m_{app} with respect to the parameters of the BRDF model: $R_{\text{spec}(i)}$, $R_{\text{diff}(i)}$, $n_{u(i)}$, and $n_{v(i)}$. The magnitudes of these scalar derivatives indicate the sensitivity of estimation algorithms based on light curve data to mismodeled surface properties.

After differentiating the model equations of Section II, the partial derivative of brightness with respect to the generic model parameter p is

$$\frac{\partial m_{\text{app}}}{\partial p} = \frac{-2.5}{\ln(10) \sum_{i=1}^N F_{\text{obs}(i)}} \sum_{i=1}^N \frac{F_{\text{obs}(i)}}{\rho_{\text{total}(i)}} \frac{\partial \rho_{\text{total}(i)}}{\partial p} \quad (22)$$

If one assumes that light is reflected from only a single facet, the summations disappear and $F_{\text{obs}(i)}$ cancels. Next, the individual parameters are substituted into the derivative expressions, and terms are grouped to determine the partial derivatives with respect to each parameter. For $p = R_{\text{spec}(i)}$, $R_{\text{diff}(i)}$, $n_{u(i)}$, and $n_{v(i)}$, respectively, this works out to

$$\frac{\partial m_{\text{app}}}{\partial R_{\text{spec}(i)}} = \frac{-2.5}{\ln(10) \rho_{\text{total}(i)}} \left\{ \frac{\rho_{\text{spec}(i)}}{F_{\text{reflect}(i)}} \left[1 - (\mathbf{u}_{\text{sun}}^I \cdot \mathbf{u}_h^I)^5 \right] - \frac{\rho_{\text{diff}(i)}}{(1 - R_{\text{spec}(i)})} \right\} \quad (23a)$$

$$\frac{\partial m_{\text{app}}}{\partial R_{\text{diff}(i)}} = \frac{-2.5}{\ln(10) \rho_{\text{total}(i)}} \frac{\rho_{\text{diff}(i)}}{R_{\text{diff}(i)}} \quad (23b)$$

$$\frac{\partial m_{\text{app}}}{\partial n_{u(i)}} = \frac{-2.5 \rho_{\text{spec}(i)}}{\ln(10) \rho_{\text{total}(i)}} \left[\frac{1}{2(n_{u(i)} + 1)} + \frac{\ln(\mathbf{u}_h^I \cdot \mathbf{u}_{n(i)}^I) (\mathbf{u}_h^I \cdot \mathbf{u}_{u(i)}^I)^2}{1 - (\mathbf{u}_h^I \cdot \mathbf{u}_{n(i)}^I)^2} \right] \quad (23c)$$

$$\frac{\partial m_{\text{app}}}{\partial n_{v(i)}} = \frac{-2.5 \rho_{\text{spec}(i)}}{\ln(10) \rho_{\text{total}(i)}} \left[\frac{1}{2(n_{v(i)} + 1)} + \frac{\ln(\mathbf{u}_h^I \cdot \mathbf{u}_{n(i)}^I) (\mathbf{u}_h^I \cdot \mathbf{u}_{v(i)}^I)^2}{1 - (\mathbf{u}_h^I \cdot \mathbf{u}_{n(i)}^I)^2} \right] \quad (23d)$$

If $n_{u(i)} = n_{v(i)} = n_{uv(i)}$, then the combination of Eqs. (23c) and (23d) simplifies to

$$\frac{\partial m_{\text{app}}}{\partial n_{uv(i)}} = \frac{-2.5 \rho_{\text{spec}(i)}}{\ln(10) \rho_{\text{total}(i)}} \left[\frac{1}{n_{uv(i)} + 1} + \ln(\mathbf{u}_h^I \cdot \mathbf{u}_{n(i)}^I) \right] \quad (24)$$

Except within a small range of attitudes near the glint direction, there is little or no specular reflection and $\rho_{\text{spec}(i)} \ll \rho_{\text{diff}(i)} \approx \rho_{\text{total}(i)}$. Consequently, several simplifications can be made. First, the sensitivities in Eqs. (23c) and (23d) are negligible and the specular parameters $n_{u(i)}$ and $n_{v(i)}$ are unobservable.

Furthermore, Eq. (23a) can be simplified as

$$\frac{\partial m_{\text{app}}}{\partial R_{\text{spec}(i)}} \approx \frac{2.5}{\ln(10)\rho_{\text{total}(i)}} \frac{\rho_{\text{diff}(i)}}{(1 - R_{\text{spec}(i)})} \quad (25)$$

which resembles the negative of Eq. (23b), especially if $R_{\text{diff}(i)} \approx 1 - R_{\text{spec}(i)}$. In other words, in the absence of significant specular reflection, a decrease in $R_{\text{diff}(i)}$ has the same effect on brightness as an increase in $R_{\text{spec}(i)}$, so the two parameters are not jointly observable. Because the fraction $\rho_{\text{diff}(i)}/\rho_{\text{total}(i)} \approx 1$ except very close to the glint region, the partial derivatives $\partial m_{\text{app}}/\partial R_{\text{spec}(i)}$ and $\partial m_{\text{app}}/\partial R_{\text{diff}(i)}$ are nearly constant outside of that region.

These qualitative characteristics can be seen in Figs. 5 and 6. Figure 5 shows the partial derivative $\partial m_{\text{app}}/\partial R_{\text{spec}(i)}$ for a range of attitudes near the glint direction, and Fig. 6 shows the partial derivative $\partial m_{\text{app}}/\partial n_{uv(i)}$ for the same attitude range, assuming that the surface is isotropic and $n_{u(i)} = n_{v(i)} = n_{uv(i)}$. Although not plotted here, $\partial m_{\text{app}}/\partial R_{\text{diff}(i)}$ is indistinguishable from the negative of $\partial m_{\text{app}}/\partial R_{\text{spec}(i)}$ in Fig. 5. The range of attitudes on the horizontal axes is the same as that of Fig. 4. Another interesting point,

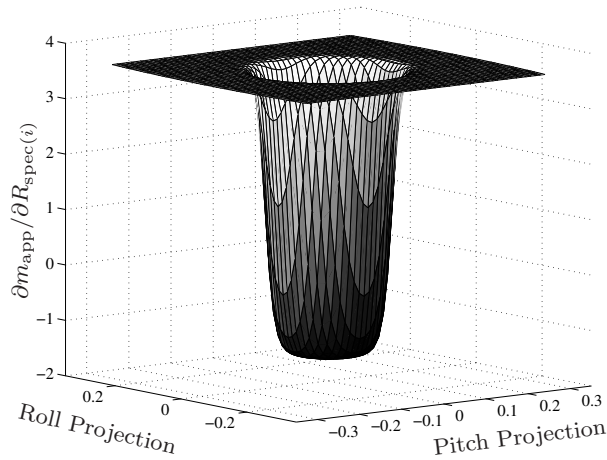


Figure 5. Partial Derivative $\partial m_{\text{app}}/\partial R_{\text{spec}(i)}$ as a Function of Attitude

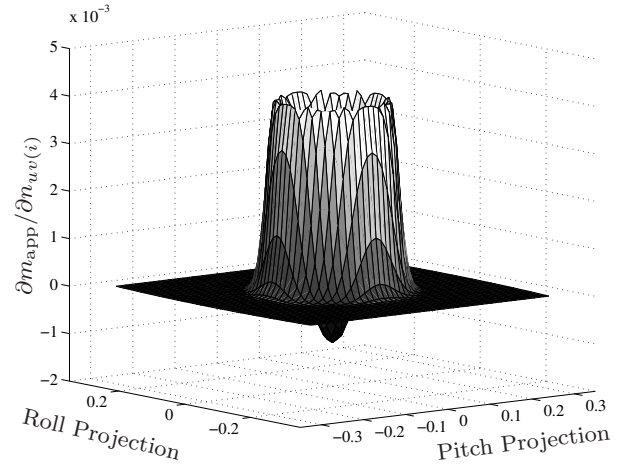


Figure 6. Partial Derivative $\partial m_{\text{app}}/\partial n_{uv(i)}$ as a Function of Attitude

which is not immediately obvious from the equations, can be seen by comparing Figs. 5 and 6 to Fig. 4 in Section IV. The vertical scales of these plots differ by several orders of magnitude. One must keep in mind, however, that a typical error in the value of $n_{uv(i)}$ would be much larger than the magnitude of the attitude error or the errors in $R_{\text{spec}(i)}$ and $R_{\text{diff}(i)}$. After accounting for such differences, the brightness m_{app} would be approximately 10 times more sensitive to typical attitude errors than to typical parameter errors. This ratio could vary significantly for different SO/Sun/observer configurations and different surface properties.

VI. Conclusions

A static observability analysis was performed to determine the attitude information available from individual light curve measurements of a space object. Analytical calculations of the single-measurement Fisher information matrix enabled the determination of its nullspace. One of the nullspace vectors lies along the body-axis surface normal vector, and an analytical expression was developed for the other, less intuitive nullspace vector. The nullspace of the Fisher information matrix indicates perturbations in attitude that are undetectable from individual measurements of apparent brightness, although such perturbations may be observable by a filter that employs a model of the space object dynamics and processes a series of measurements. The light curve model parameters are not jointly observable in the static case except when attitude is very near the glint direction.

References

- ¹Sato, T., Wakayama, T., Tanaka, T., Ikeda, K.-i., and Kimura, I., "Shape of Space Debris as Estimated from Radar Cross Section Variations," *Journal of Spacecraft and Rockets*, Vol. 31, No. 4, Oct. 1994, pp. 665–670.
- ²Walker, J. L., "Range-Doppler Imaging of Rotating Objects," *IEEE Transactions on Aerospace and Electronic Systems*, Vol. AES-16, No. 4, Jan. 1980, pp. 23–52.
- ³Hagfors, T., "Mapping of Planetary Surfaces by Radar," *Proceedings of the IEEE*, Vol. 61, No. 9, Jan. 1973, pp. 1219–1225, Piscataway, NJ.
- ⁴DiMatteo, J., Florakis, D., Weichbrod, A., and Milam, M., "Proximity Operations Testing with a Rotating and Translating Resident Space Object," *AIAA Guidance, Navigation, and Control Conference*, Aug. 2009, AIAA-2009-6293.
- ⁵Lichter, M. D. and Dubowsky, S., "State, Shape, and Parameter Estimation of Space Objects from Range Images," *Proceedings of IEEE International Conference on Robotics and Automation*, Vol. 3, April 26–May 1, 2004, pp. 2974–2979, New Orleans, LA.
- ⁶Young, G. S. J. and Chellappa, R., "3-D Motion Estimation using a Sequence of Noisy Stereo Images: Models, Estimation, and Uniqueness Results," *IEEE Transactions on Pattern Analysis and Machine Intelligence*, Vol. 12, No. 8, 1990, pp. 735–759.
- ⁷Broida, T. J. and Chellappa, R., "Estimating the Kinematics and Structure of a Rigid Object from a Sequence of Monocular Images," *IEEE Transactions on Pattern Analysis and Machine Intelligence*, Vol. 13, No. 6, 1991, pp. 497–513.
- ⁸Kaasalainen, M. and Torppa, J., "Optimization Methods for Asteroid Lightcurve Inversion I: Shape Determination," *Icarus*, Vol. 153, No. 4, Jan. 2001, pp. 24–36.
- ⁹Kaasalainen, M. and Torppa, J., "Optimization Methods for Asteroid Lightcurve Inversion II: The Complete Inverse Problem," *Icarus*, Vol. 153, No. 4, Jan. 2001, pp. 37–51.
- ¹⁰Calef, B., Africano, J., Birge, B., Hall, D., and Kervin, P., "Photometric Signature Inversion," *Proceedings of the Intl. Society for Optical Engineering (SPIE) 6307*, Sept. 2006, Unconventional Imaging II, San Diego, CA.
- ¹¹Jah, M. and Madler, R., "Satellite Characterization: Angles and Light Curve Data Fusion for Spacecraft State and Parameter Estimation," *Proceedings of the Advanced Maui Optical and Space Surveillance Technologies Conference*, Vol. 49, Sept. 2007, Wailea, Maui, HI, Paper E49.
- ¹²Centinello, F. J., "Six Degree of Freedom Estimation with Light Curve Data," Tech. rep., AFRL, Kihei, HI, 2008, Tech. Report.
- ¹³Shuster, M. D. and Oh, S. D., "Three-Axis Attitude Determination from Vector Observations," *Journal of Guidance and Control*, Vol. 4, No. 1, Jan.-Feb. 1981, pp. 70–77.
- ¹⁴Shuster, M. D., "Maximum Likelihood Estimation of Spacecraft Attitude," *Journal of the Astronautical Sciences*, Vol. 37, No. 1, Jan.-March 1989, pp. 79–88.
- ¹⁵Lefferts, E. J., Markley, F. L., and Shuster, M. D., "Kalman Filtering for Spacecraft Attitude Estimation," *Journal of Guidance, Control, and Dynamics*, Vol. 5, No. 5, Sept.-Oct. 1982, pp. 417–429.
- ¹⁶Slama, C. C., editor, *Satellite Photogrammetry*, chap. 17, Manual of Photogrammetry, American Society of Photogrammetry, Falls Church, VA, 4th ed., 1980.
- ¹⁷Ashikmin, M. and Shirley, P., "An Anisotropic Phong Light Reflection Model," Tech. Rep. UUCS-00-014, University of Utah, Salt Lake City, UT, 2000.
- ¹⁸Ashikmin, M. and Premoze, S., "Distribution-Based BRDFs," 2007, Unpublished Tech. Report, University of Utah.
- ¹⁹Schlick, C., "An Inexpensive BRDF Model for Physically-Based Rendering," *Computer Graphics Forum*, Vol. 13, No. 3, 1994, pp. 233–246.
- ²⁰Crassidis, J. L. and Junkins, J. L., *Optimal Estimation of Dynamic Systems*, Chapman & Hall/CRC Press, Boca Raton, FL, 2nd ed., 2011, pp. 81–86.